

Surface phase diagrams for the Ag–Ge(111) and Au–Si(111) systems

D. Grozea, E. Bengu, L.D. Marks *

Department of Materials Science and Engineering, Northwestern University, Evanston, IL 60208, USA

Received 20 December 1999; accepted for publication 13 March 2000

Abstract

Based on results from recent structural studies and an overview of the literature, we propose surface phase diagrams for the Au–Si(111) system in the supermonolayer regime and for the Ag–Ge(111) system in the submonolayer region. In addition, time–temperature–transformation (T–T–T) curves are proposed to represent the metastable structures present in surface phase systems. © 2000 Elsevier Science B.V. All rights reserved.

Keywords: Germanium; Gold; Metallic films; Metal–semiconductor interfaces; Silicon; Silver; Surface relaxation and construction

1. Introduction

Surface phase diagrams provide fundamental understanding of surface and interface phenomena, and can be used to predict the effects of changing parameters such as temperature or metal coverage on the atomic arrangement of surface structures. They also provide the starting point for understanding the kinetics of phase transitions at surfaces. However, to date there have been relatively few studies of the phase diagrams for simple metals on semiconductors where the basic Gibbs phase rules have been applied; instead, ‘phase maps’ summarizing the conditions of temperature and coverage have been used. In many cases these phase maps necessarily contain errors; for instance, unless a particular phase contains sites with variable occupancy, i.e. is a ‘surface solution’, almost without exception it can only occur in combination

with another, in what is called two-phase coexistence.

The thermodynamic phase diagram of a particular system is what it will achieve if held for very long times at the specified temperatures. However, kinetic effects must also be considered. The analysis of experimental results for a certain system can be complicated by the presence of metastable phases, due mostly to kinetic effects, or by incomplete phase transitions. We propose here the use of a set of curves commonly referred to in physical metallurgy as time–temperature–transformation (T–T–T) curves as a way to represent the metastable structures that may be present in surface phase systems [1]. The T–T–T curves provide information on the time that elapses, at any selected temperature, before the transformation begins and until it is finished. When an alloy is continuously and slowly cooled, most of the transformation occurs at high temperature, whereas at a fast continuous cooling rate most of the transformation occurs at low temperatures. The ‘start’ and ‘finish’ lines are usually defined as the moments when 1% of the

* Corresponding author. Fax: +1-847-491-7820.
E-mail address: ldm@apollo.numis.nwu.edu (L.D. Marks)

parent phase has transformed and when 99% of the transformation has occurred respectively.

Based on the atomic arrangement of all phases present and the interphase relationships, we report here a survey of the results of all relevant experimental reports and tentative surface phase diagrams for the Ag–Ge(111) system in the submonolayer regime and the Au–Si(111) system in the supermonolayer regime.

2. Background for Au–Si (111) and Ag–Ge (111)

An overview of the literature on thin metal deposits on clean semiconductor surfaces, in particular for the Au–Si(111) and Ag–Ge(111) systems, shows a great difference in the number of studies. Although the Au–Si(111) interface is one of the most extensively investigated, for the Ag–Ge(111) system the available information is, at best, fragmentary. A complete understanding of surface phenomena in metal–semiconductor systems requires knowledge of the atomic arrangement. Recently, several reports have provided this information for the Au–Si(111) surface structures in the supermonolayer region of the system (Au coverage up to 1.5 ML) [2–5], and for the Ag–Ge(111) system in the submonolayer regime [6–10].

Solving the atomic structure for the two main surface phases of the Au–Si(111) system in the submonolayer regime, (5×2) Au and $(\sqrt{3} \times \sqrt{3})$ Au, in conjunction with results from numerous recent studies on this system allowed Plass and Marks [11,12] to propose a phase diagram obeying the Gibbs phase rule as shown in Fig. 1. Their analysis was limited to the submonolayer region, although Fig. 1 encompasses experimental observations from the literature up to 2 ML of Au coverage. The data points have errors of at least ± 0.04 ML on the Au coverage and $\pm 20^\circ\text{C}$ on temperature. The estimation is based on typical limitations of quartz monitors, Auger electron spectroscopy (AES), and Rutherford backscattering for coverage measurements, and of pyrometers for temperature measurements. They redefined the reconstructions in terms of ‘line compounds’ or

‘surface solutions’. As both (5×2) Au and $(\sqrt{3} \times \sqrt{3})$ Au phases can sustain varying Au contents, they are considered surface solutions.

Another important point from their analysis is the distinction between studies reporting structural observations at the same temperature at which the structure formed and investigations in which the structure was observed at a lower temperature than the formation temperature. Both data sets follow the same general trends provided that the larger coverage and temperature uncertainties in the latter data set are considered. This separation can be taken into account when analyzing the supermonolayer regime of Au–Si(111), and this study will focus mostly on the former types of experimental observation. However, the majority of Ag–Ge(111) observations were performed at a lower temperature than the phase formation temperature. At least for this case, there are no reported differences between structures formed when the metal is deposited on a heated substrate and those induced on the surface by annealing the system after the metal is deposited at room temperature [9,10].

One assumption required for a sound thermodynamic evaluation is that the system studied is closed with respect to the amount of its constituents. Surface diffusion can occur simultaneously with competitive processes like desorption and bulk diffusion. For the case of the Au–Si(111) system, under certain temperature and Au coverage conditions, the surface migration process takes place simultaneously with the diffusion of Au atoms into the bulk. Yuhara et al. [20] reported an activation energy of 1.3 eV for Au atoms diffusing into bulk Si for Au coverages of around 1.7 ML, with an increase to 2.5 ± 0.5 eV for Au diffusion from the $\alpha(\sqrt{3} \times \sqrt{3})$ surface at moderate temperatures (between 400 and 600°C). Desorption starts to play a role at temperatures over 800°C. Le Lay et al. [30] determined, based on AES data, that the desorption energies of Au atoms from structures with Au coverages greater than 1 ML and from the $\alpha(\sqrt{3} \times \sqrt{3})$ surface are 3.3 eV and 3.6 eV respectively.

Suliga and Henzler [31] claimed, in contrast to the Au–Si(111) system, no significant Ag diffusion

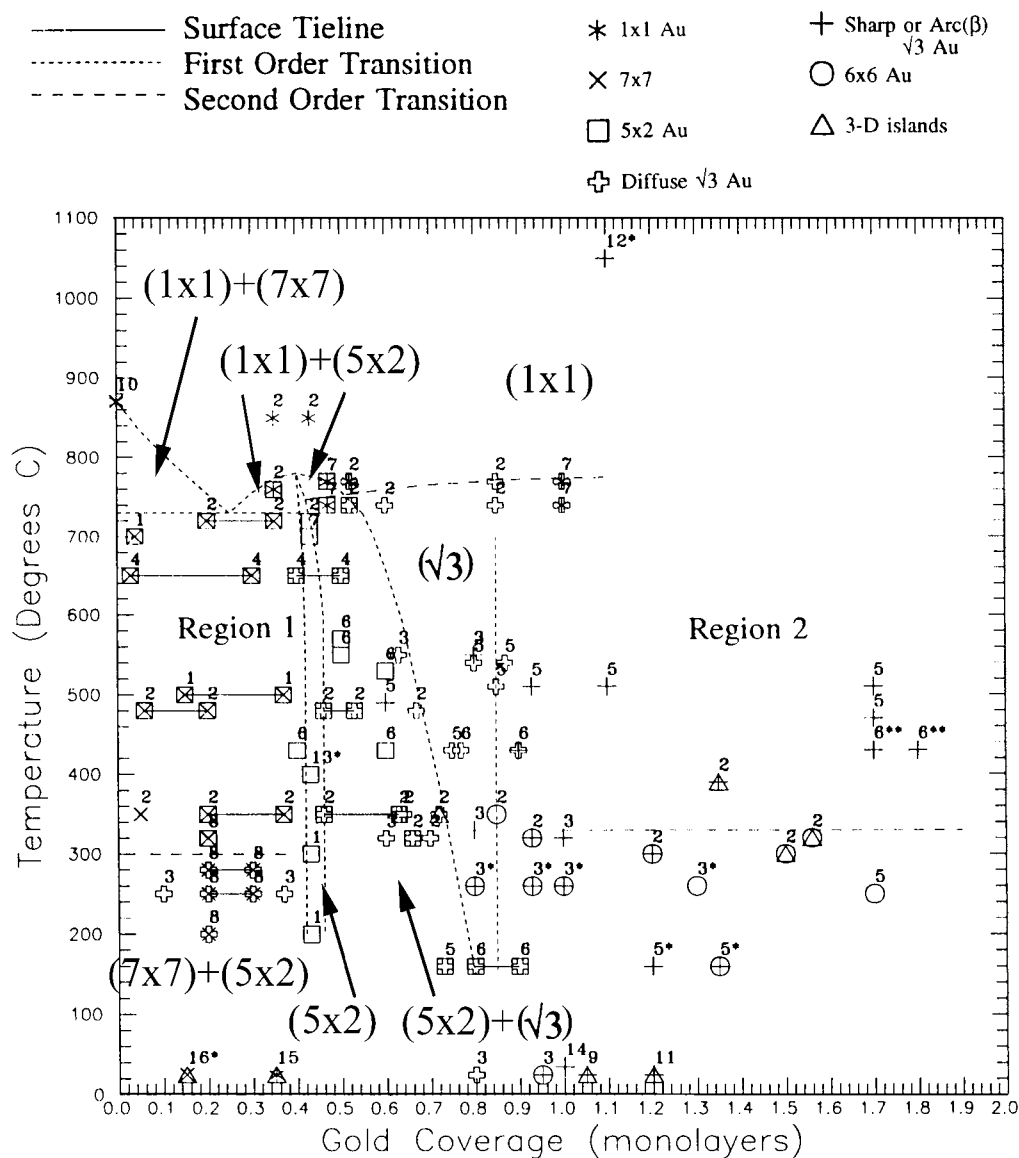


Fig. 1. Surface phase diagram for the Au–Si(111) system proposed by Plass [12] (Region 1 — submonolayer coverage) with in situ experimental results. Region 2 (1–2 ML coverage) displays experimental data points. Data points taken from coverage estimates based on the references' images have starred (*) reference numbers. The number above a data point corresponds to its reference as follows: 1, Hasegawa and coworkers [13–15]; 2, Świąch et al. [16]; 3, Takahashi et al. [17]; 4, Tanishiro and Takayanagi [18]; 5, Yuhara et al. [19]; 6, Yuhara et al. [20]; 7, Daimon et al. [21]; 8, Shibata et al. [22]; 9, Fuchigami and Ichimiya [23]; 10, Miki et al. [24]; 11, Ichimiya et al. [25]; 12, Kamino et al. [26]; 13, Minoda et al. [27]; 14, Plass [12]; 15, Berman et al. [28]; 16, Meinel and Katzer [29].

into bulk Ge for the Ag–Ge(111) system under 1 ML coverage. Silver atoms on the Ge(111) surface start to desorb at around 550–600°C. Therefore, both systems under investigation, Au–

Si(111) and Ag–Ge(111), can be considered closed, a reasonable approximation within a certain temperature range, metal coverage, and duration of heating.

3. The Ag–Ge(111) system

When Ag is deposited on the Ge(111) native reconstruction [the Ge(111)-c(2×8) surface], the interface undergoes a (3×1) Ag, a (4×4) Ag, and eventually a ($\sqrt{3}\times\sqrt{3}$)R30° Ag reconstruction at a substrate temperature of between 200 and 450°C in the submonolayer regime. For Ag coverages above 0.1 ML, a (4×4) phase is observed, initially coexisting with the c(2×8) surface. This phase was first reported to be complete at 0.27 ML [32] and later at 0.375 ML [6,10]. Hammar et al. [33] identified for the first time a (3×1) structure existing only as small insets at the boundaries of the (4×4) and c(2×8) phase domains. Grozea et al. [7] reported the existence and stability of the (3×1) phase over large areas and with a nominal coverage of 0.33 ML. Upon further deposition of Ag, the (4×4) structure gradually disappears and is replaced by a ($\sqrt{3}\times\sqrt{3}$) phase, which appears to cover completely the surface at 1 ML.

The ($\sqrt{3}\times\sqrt{3}$) phase has a honeycomb-chained trimer structure [8–10] similar to that of the ($\sqrt{3}\times\sqrt{3}$) surface in the Ag–Si(111) system [34]. The reconstruction can be described as a missing top layer, in which Ag atoms substitute the first-layer Ge atoms in positions slightly displaced from bulk sites while the remaining Ge atoms in the topmost double layer form trimers. The correspondence between atomic models for (3×1) and ($\sqrt{3}\times\sqrt{3}$) structures of Ag on both Si(111) and Ge(111) can account for a similar link between the two structures on Ge(111) as on Si(111) [35]. This points to a similar local bonding geometry, in which each Ag atom bonds most strongly to a single semiconductor atom from the semiconductor chain and has two other atoms surrounding it in the (3×1) phase and, in the ($\sqrt{3}\times\sqrt{3}$) phase, the Ag atom bonds most strongly to a single semiconductor atom from the trimer and has two others as neighbors.

The (3×1) surface can be described as a partial Ge double layer containing a Ge chain and one missing row, leaving a trench in which the Ag atoms lie [7]. There are two equivalent Ag positions, with the Ag atoms shifted in the same direction for rows parallel to the trench. In addition,

a theoretical study by Erwin and Weiering [36] proposed the existence of a true semiconductor double bond for the (3×1) reconstruction as an explanation for the model's stability.

The (4×4) surface consists of a missing top layer reconstruction with the Ag atoms placed on Ge substitutional sites in one triangular subunit. The other triangular subunit contains a ring-like assembly of Ge atoms with double bonds eliminating all the dangling bonds and contributing to the ring's stability. The formation of this unusual Ge=Ge double bond is a feature shared with the (3×1) phase. The (4×4) structure also has trimers of Ge atoms, similar to the trimers found on the ($\sqrt{3}\times\sqrt{3}$) surface, at the corners of the unit cell [6]. The Ge trimer with the three nearest Ag atom neighbors matches the basic structural unit of the ($\sqrt{3}\times\sqrt{3}$) phase. The partially occupied Ag sites included by Collazo-Davila et al. [6] in their final model suggest that the (4×4) phase is a surface solution with a lower coverage boundary at 0.375 ML and an upper coverage boundary of 0.5625 ML.

Bertucci et al. [32] proposed a kinetic model of desorption for the (4×4) and ($\sqrt{3}\times\sqrt{3}$) structures, in which desorption is assumed to occur indirectly through surface diffusion from the domain edge. Their model resulted in sublimation energies of 2.93 eV and 3.3 eV for ($\sqrt{3}\times\sqrt{3}$) and (4×4) respectively.

The similarity between the Ag–Ge(111) and Ag–Si(111) surfaces extends to the energies for adsorption E_a , binding E_b , and diffusion E_d processes on top of the ($\sqrt{3}\times\sqrt{3}$) layers for both systems, with E_d+3E_b in the range of 0.55–0.60 eV [37]. (The theoretical nucleation density on a perfect surface is proportional to $\exp(E/kT)$, where E for Ag on Ge(111) and Si(111) is $E=E_d+3E_b$.)

Both Suliga and Henzler [31] and Metcalfe and Venables [38] note an instability of the ($\sqrt{3}\times\sqrt{3}$) layer upon annealing at 350°C. Metcalfe and Venables [38] observed patches of ($\sqrt{3}\times\sqrt{3}$) areas that, during annealing (even if the overall patch width increases), split into two regions: an inner region corresponding to the ($\sqrt{3}\times\sqrt{3}$) structure, and an outer region of a lower coverage, corre-

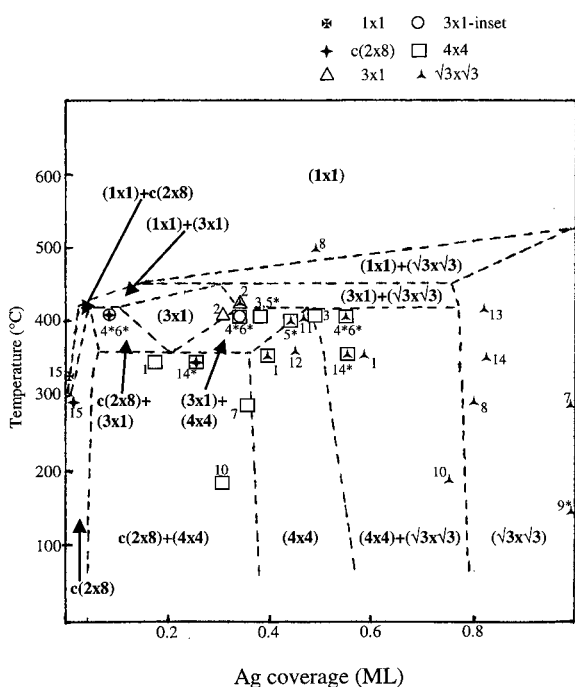


Fig. 2. Proposed surface phase diagram for the Ag–Ge(111) system in the submonolayer regime with experimental data points. The number above a data point corresponds to its reference as follows: 1, Spence and Tear [10]; 2, Grozea et al. [7]; 3, Collazo-Davila et al. [6]; 4, Weiting and Carpinelli [39]; 5, Göthelid et al. [9]; 6, Hammar et al. [33]; 7, Metcalfe and Venables [38]; 8, Huang et al. [8]; 9, Dornisch et al. [40]; 10, Busch and Henzler [41]; 11, Fan and Ignatiev [42]; 12, Knapp et al. [43]; 13, Suliga and Henzler [31]; 14, Bertucci et al. [32]; 15, Phaneuf and Webb [44].

sponding to the (4×4) structure. This effect is coupled with a rapid diffusion of Ag atoms over the (4×4) structure. The activation energies for the spreading of the $(\sqrt{3} \times \sqrt{3})$ and the (4×4) phases were estimated as 0.78 eV and 0.87 eV respectively.

A new phase diagram for the Ag–Ge(111) system in the submonolayer regime is shown in Fig. 2, based on available data points from the literature and the principles used for constructing binary phase diagrams. Although this diagram can explain all of the experimental observations for this system, it should be noted that it is provisional, at best, without further computational supporting evidence. However, even the application of thermodynamic calculations for the determination

of conventional binary phase diagrams for bulk systems is not yet fully feasible. The dashed curves represent potential phase boundaries that have not been derived from energy parameters. They are drawn to accommodate the experimental reports. The curves show first-order, reversible transitions between the surface phases. Single symbols represent a reported surface completely covered by one surface structure. Overlapping symbols show the presence on the surface of several structures at the same time.

The existence of the peritectoid region at very low Ag coverages can be inferred from the reversible transition from the $c(2 \times 8)$ phase to a (1×1) phase at 300°C [44], coupled with observations of the $c(2 \times 8)$ and the (4×4) phases occurring simultaneously on the surface at 350°C (Bertucci et al. [32] — one of the only studies that made observations at the phase formation temperature, 350°C) or with small insets of the (3×1) phase separating $c(2 \times 8)$ domains and the (4×4) domains at 350°C [10] and 400°C [33,39]. No traces of Ag were observed on the $c(2 \times 8)$ terraces, and at no point was the $c(2 \times 8)$ phase observed to coexist with the $(\sqrt{3} \times \sqrt{3})$ structure [33,39].

The (3×1) phase observations can be separated into two categories. Only one study [7] reported its presence over a large area of the surface, and, in another experiment, coexisting with the $(\sqrt{3} \times \sqrt{3})$ phase. The second type of observation includes the small insets of the (3×1) surface, and it is shown using a different symbol. In addition to being observed bordering $c(2 \times 8)$ and (4×4) domains, the (3×1) was also reported as separating large (4×4) domains [33]. The narrow temperature range over which the (3×1) structure covers large areas of the surface reflects the fact that only one study was able to match the necessary observation conditions. The experimental data suggest that the $c(2 \times 8)$, (3×1) , and (4×4) phases may be related by a eutectoid region; the position of the eutectoid point was arbitrarily selected.

4. The Au–Si(111) system

The groundwork for extending the phase diagram of the Au–Si(111) system to the supermono-

layer regime (up to 1.5 ML) has been laid out by the work of Plass [12]. Fig. 1 shows all the results pertaining to this problem. The experimental observations mapped in Fig. 1 are used as the basis of this study. Plass [12] did not attempt to extend his phase diagram representation to the supermonolayer regime since crucial pieces of information, particularly the atomic geometry of the $\beta(\sqrt{3} \times \sqrt{3})$ and (6×6) phases and the relationships between them, were not available.

The Au–Si(111) supermonolayer interfaces are reported to be reconstructed into $\alpha(\sqrt{3} \times \sqrt{3})$, $\beta(\sqrt{3} \times \sqrt{3})$, and (6×6) structures, depending on the annealing conditions and the amount of Au deposited. In addition, the picture is complicated by the presence of small Au particles that nucleate and grow at various temperatures. They were reported [16] to occur even before the (6×6) structure formation and continue to appear in parallel with that reconstruction. The small particles were also observed at higher temperatures on the same surface with the $\beta(\sqrt{3} \times \sqrt{3})$ structure (our own experiments and those of Świąch et al. [16]).

The atomic structure of the $\alpha(\sqrt{3} \times \sqrt{3})$ phase, which occurs up to 0.95–1.0 ML, consists of sets of Au and Si trimers in the top two layers, forming a missing top layer twisted trimer structure [3]. The $\alpha(\sqrt{3} \times \sqrt{3})$ displays a diffraction pattern with diffuse spots. Okuda et al. [45] reported SCLS (Surface Core Level Shift) data showing a spectral dissimilarity between the $\alpha(\sqrt{3} \times \sqrt{3})$ and the $\beta(\sqrt{3} \times \sqrt{3})$ structures and a strong resemblance between $\beta(\sqrt{3} \times \sqrt{3})$ and (6×6) phases. Based on these results, it can be said that the chemical environments of topmost Si atoms of the $\alpha(\sqrt{3} \times \sqrt{3})$ and $\beta(\sqrt{3} \times \sqrt{3})$ differ from each other and that a distinction between these two surfaces is necessary. In agreement with scanning tunneling microscopy observations [46], the angle-resolved photoelectron spectroscopy measurements of Okuda et al. [45] are consistent with a smaller density of the domain walls on the $\alpha(\sqrt{3} \times \sqrt{3})$ surface than on the $\beta(\sqrt{3} \times \sqrt{3})$ and (6×6) surfaces, which again look similar.

The structure modeling of the (6×6) phase and its disordered form, $\beta(\sqrt{3} \times \sqrt{3})$, was presented in Refs. [4,5]. Briefly, the atomic arrangement on the

(6×6) surface can be described as microdomains of the parent $(\sqrt{3} \times \sqrt{3})$ Au structure. A better description is in terms of a tiling of incomplete pentagonal and trimer units (or as a combination of two Au ring structures, A and B, surrounding three Si atoms in the next layer, with two rotational variants of B), essentially a pseudo-pentagonal glass. The possibility of varying its content from 1.2 to 1.5 ML (by completing the pentagons and by filling the centers of the B-type rings) denotes it as a surface solution.

The $\beta(\sqrt{3} \times \sqrt{3})$ and the (6×6) phases form at the same Au coverage. The $\beta(\sqrt{3} \times \sqrt{3})$ structure corresponds to a glass-like tiling using A and B ring structures sitting at $(\sqrt{3} \times \sqrt{3})$ lattice sites and giving a diffraction pattern with sharp spots surrounded by ring-like features. Because the movement of the A and B units is expected to be very slow compared with that of single atoms, it is understandable that the transition between $\beta(\sqrt{3} \times \sqrt{3})$ and (6×6) surfaces behaves like a glass transition in requiring low temperature annealing and large mass transport for the formation of the ‘crystalline’ phase.

The proposed phase diagram extension from 1.0 to 1.5 ML for the Au–Si(111) system is shown in Fig. 3, with the same considerations mentioned for Figs. 1 and 2. A eutectoid point, arbitrarily chosen, seems to exist between the $\beta(\sqrt{3} \times \sqrt{3})$ phase, the three-dimensional particles region, and the high-temperature phase. More experiments are necessary to configure the high-temperature ‘uncharted territory’ and define the phase boundaries for regions such as $\alpha(\sqrt{3} \times \sqrt{3}) + (1 \times 1)$ and $\beta(\sqrt{3} \times \sqrt{3}) + (1 \times 1)$.

There are a number of alloy systems, such as Cu–Au, that display a similar behavior as the order–disorder transformation observed between the (6×6) and $\beta(\sqrt{3} \times \sqrt{3})$ phases. A disordered phase is present above a certain temperature and is transformed to an ordered phase when it reaches equilibrium at lower temperatures. Since the change takes place by diffusion, the rapid cooling of the system can suppress the transformation. However, the reverse change, from the ordered phase to the disordered one, cannot be avoided. By analogy with the Cu–Au system, where an

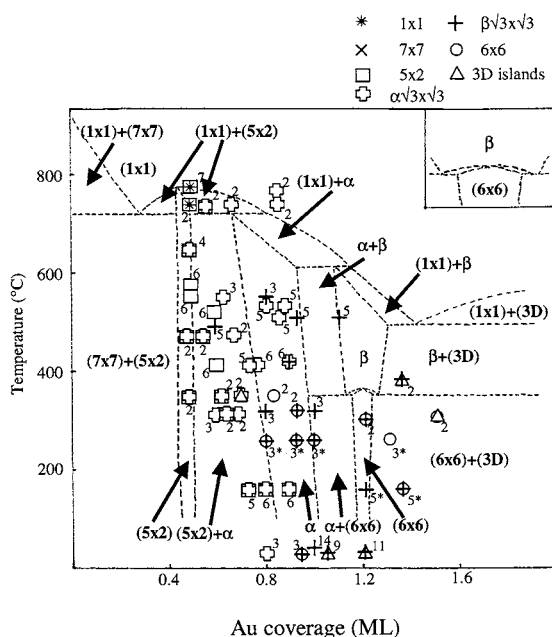


Fig. 3. Proposed phase diagram extension to the supermonolayer regime for the Au–Si(111) system with experimental data points, limited from 0.5 to 1.5 ML, from Fig. 1. Inset: a magnified view of the region where the order–disorder transformation occurs.

ordered phase forms from the disordered phase through a congruent transformation at the stoichiometric composition and with a eutectoid transformation at the Au-rich side, a similar transition is proposed from the $\beta(\sqrt{3} \times \sqrt{3})$ phase to the (6×6) phase. The rate of the ordering reaction follows a T–T–T curve, shown in Fig. 4. The exact

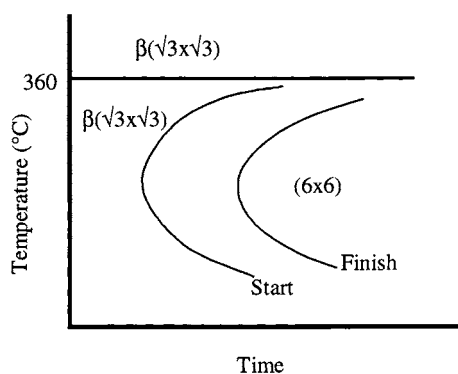


Fig. 4. T–T–T curve representation of the transformation from $\beta(\sqrt{3} \times \sqrt{3})$ phase to the (6×6) phase.

start and finish positions are yet to be determined, but Fig. 4 qualitatively explains the experimental data and the transformation analysis very well.

5. Discussion

In this study, we have applied the long-standing principles of physical metallurgy to the study of surface phases. The use of T–T–T curves to explain kinetically constrained phases and represent the evolution of the phase transformation with a family of curves showing different percentages of completion appears to be beneficial, although more work is required to determine the details. Since the surface phases seem to obey the same general principles as their bulk counterparts, the introduction of T–T–T curves into surface system analysis adds to this analogy. It is also important to note that T–T–T diagrams are not equilibrium diagrams in the sense that phase diagrams are. However, the far right side of the T–T–T plot represents extended periods of time; consequently, there should be a match between that region and the phase diagram in terms of the phases present.

Any attempt to progress from simple phase maps to true surface phase diagrams, with phase boundaries based on thermodynamic principles, must be supported by determining the structure of the system's phases. This proved to be the case for the extension of the phase diagram of the Au–Si(111) system from 1 ML up to 1.5 ML and partially into the region where nanoparticles coexist with surface reconstructions. The key point was the knowledge of the (6×6) and $\beta(\sqrt{3} \times \sqrt{3})$ structural features and the relationships between the two structures. An extended investigation of this system is still necessary to confirm that the order–disorder transition between high coverage structures is a first-order transformation with definite two-phase fields and eutectoid points on each side.

In addition to the solution of the atomic arrangement of the (3×1) and (4×4) phases, the understanding of the links between all three phases present in the submonolayer coverage regime plays an important role in constructing the proposed Ag–Ge(111) system phase diagram.

Considering the bulk phase diagrams of the Au–Si(111) and Ag–Ge(111) systems, an interesting comparison regarding the thermal stability of metal-covered surfaces at low and higher metal coverages can be made. Au–Si shows a deep eutectic in contrast to Ag–Ge. In the Au–Si(111) system, the (6×6) phase becomes unstable at temperatures around the Au–Si bulk eutectic temperature; however, the Ag–Ge(111) surface displays a decrease in stability toward low coverages.

As the next step, more experiments are needed to confirm some of the phase boundaries proposed in these preliminary phase diagrams as well as the presence and position of the eutectoid/peritectoid points.

Acknowledgement

This work was supported by the National Science Foundation on grant number DMR-9214505.

References

- [1] C.R. Barrett, W.D. Nix, A.S. Tetelman, *The Principles of Engineering Materials*, Prentice-Hall, Englewood Cliffs, NJ, 1973.
- [2] L.D. Marks, R. Plass, *Phys. Rev. Lett.* 75 (1995) 2172.
- [3] R. Plass, L.D. Marks, *Surf. Sci.* 342 (1995) 233.
- [4] D. Grozea, E. Landree, L.D. Marks, R. Feidenhans'l, M. Nielsen, R.L. Johnson, *Surf. Sci.* 418 (1998) 32.
- [5] L.D. Marks, D. Grozea, R. Feidenhans'l, M. Nielsen, R.L. Johnson, *Surf. Rev. Lett.* 5 (1998) 459.
- [6] C. Collazo-Davila, D. Grozea, L.D. Marks, R. Feidenhans'l, M. Nielsen, L. Seehofer, L. Lottermoser, G. Falkenberg, R.L. Johnson, M. Göthelid, U. Karlsson, *Surf. Sci.* 418 (1998) 395.
- [7] D. Grozea, E. Bengu, C. Collazo-Davila, L.D. Marks, *Surf. Rev. Lett.* (1999) in press.
- [8] H. Huang, H. Over, S.Y. Tong, J. Quinn, F. Jona, *Phys. Rev. B* 49 (1994) 13483.
- [9] M. Göthelid, M. Hammar, U.O. Karlsson, C. Wigren, G. Le Lay, *Phys. Rev. B* 52 (1995) 14104.
- [10] D.J. Spence, S.P. Tear, *Surf. Sci.* 398 (1998) 91.
- [11] R. Plass, L.D. Marks, *Surf. Sci.* 380 (1997) 497.
- [12] R. Plass, *Gold induced Si(111) surface reconstructions studied by ultrahigh vacuum transmission electron microscopy*, Ph.D. Thesis dissertation, Northwestern University, Illinois, 1996.
- [13] T. Hasegawa, K. Takata, S. Hosaka, S. Hosoki, *J. Vac. Sci. Technol. B*: 9 (1991) 758.
- [14] T. Hasegawa, S. Hosaka, S. Hosoki, *Jpn. J. Appl. Phys.* 31 (1992) L1492.
- [15] T. Hasegawa, S. Hosaka, S. Hosoki, *Surf. Sci.* 358 (1996) 858.
- [16] W. Świąch, E. Bauer, M. Mundschau, *Surf. Sci.* 253 (1991) 283.
- [17] S. Takahashi, Y. Tanishiro, K. Takayanagi, *Surf. Sci.* 242 (1991) 73.
- [18] Y. Tanishiro, K. Takayanagi, *Ultramicroscopy* 27 (1989) 1.
- [19] J. Yuhara, M. Inoue, K. Morita, *J. Vac. Sci. Technol. A*: 10 (1992) 334.
- [20] J. Yuhara, M. Inoue, K. Morita, *J. Vac. Sci. Technol. A*: 10 (1992) 3486.
- [21] H. Daimon, C. Chung, S. Ino, Y. Watanabe, *Surf. Sci.* 235 (1990) 142.
- [22] A. Shibata, Y. Kimura, K. Takayanagi, *Surf. Sci.* 273 (1992) L430.
- [23] K. Fuchigami, A. Ichimiya, *Surf. Sci.* 357–358 (1996) 937.
- [24] K. Miki, Y. Morita, H. Tokumoto, T. Sato, M. Iwatsuki, M. Suzuki, T. Fukuda, *Ultramicroscopy* 42 (1992) 851.
- [25] A. Ichimiya, H. Nomura, Y. Ito, H. Iwashige, *J. Cryst. Growth* 150 (1995) 1169.
- [26] T. Kamino, T. Yaguchi, M. Tomita, H. Saka, *Philos. Mag. A*: 75 (1996) 105.
- [27] H. Minoda, Y. Tanishiro, N. Yamamoto, K. Yagi, *Appl. Surf. Sci.* 60 (1992) 107.
- [28] L.E. Berman, B.W. Batterman, J.M. Blakely, *Phys. Rev. B* 38 (1988) 5397.
- [29] K. Meinel, D. Katzer, *Appl. Surf. Sci.* 56–58 (1992) 514.
- [30] G. Le Lay, M. Manneville, R. Kern, *Surf. Sci.* 65 (1977) 261.
- [31] E. Suliga, M. Henzler, *J. Phys. C*: 16 (1983) 1543.
- [32] M. Bertucci, G. Le Lay, M. Manneville, R. Kern, *Surf. Sci.* 85 (1979) 471.
- [33] M. Hammar, M. Göthelid, U.O. Karlsson, S.A. Flodström, *Phys. Rev. B* 47 (1993) 15669.
- [34] T. Takahashi, S. Nakatani, *Surf. Sci.* 282 (1993) 17.
- [35] C. Collazo-Davila, D. Grozea, L.D. Marks, *Phys. Rev. Lett.* 80 (1998) 1678.
- [36] S.C. Erwin, H.H. Weitering, *Phys. Rev. Lett.* 81 (1998) 2296.
- [37] J.A. Venables, F.L. Metcalfe, A. Sugawara, *Surf. Sci.* 371 (1997) 420.
- [38] F.L. Metcalfe, J.A. Venables, *Surf. Sci.* 369 (1996) 99.
- [39] H.H. Weitering, J.M. Carpinelli, *Surf. Sci.* 384 (1997) 240.
- [40] D. Dornisch, W. Moritz, H. Schulz, R. Feidenhans'l, M. Nielsen, F. Grey, R.L. Johnson, G. Le Lay, *Surf. Sci.* 274 (1992) 215.
- [41] H. Busch, M. Henzler, *Phys. Rev. B* 41 (1990) 4891.
- [42] W.C. Fan, A. Ignatiev, *Phys. Rev. B* 40 (1989) 5479.
- [43] B.J. Knapp, J.C. Hansen, M.K. Wagner, W.D. Clendening, J.G. Tobin, *Phys. Rev. B* 40 (1989) 2814.
- [44] R.J. Phaneuf, M.B. Webb, *Surf. Sci.* 164 (1985) 167.
- [45] T. Okuda, H. Daimon, S. Suga, Y. Tezuka, S. Ino, *Appl. Surf. Sci.* 121–122 (1997) 89.
- [46] J. Nogami, A.A. Baski, C.F. Quate, *Phys. Rev. Lett.* 65 (1990) 1611.